Methodological proposal to assess plastic greenhouses land cover change from the combination of archival aerial orthoimages and Landsat data

Óscar González-Yebra*, Manuel A. Aguilar, Abderrahim Nemmaoui, Fernando J. Aguilar

Department of Engineering, University of Almerí, Ctra. de Sacramento s/n 04120, La Cañada de San Urbano, Almería, Spain (https://doi.org/10.1016/j.biosystemseng.2018.08.009)

Abstract

This work outlines a methodological proposal to assess Plastic Covered Greenhouses (PCG) land cover change from the combination of archival aerial orthoimages and Landsat data. Moreover, landscape spatial metrics were semi-automatically derived for applying on the analysis of the spatial arrangement of PCG areas. The experimental process consisted of two main phases: (i) Mapping PCG through a semi-automatic Object-Based Image Analysis (OBIA) approach relying on segmentation plus non-parametric supervised classification; (ii) Processing the obtained PCG classified objects to yield different landscape spatial metrics. The case study has focused on two high dense PCG sites located in southeastern Spain. To analyse PCG land cover evolution, each study site was composed of three multi-temporal remote sensed datasets formed by the fusion of orthoimages (O) derived from archival aerial photography and temporally corresponding Landsat images (L). In terms of PCG mapping performance, the best results were obtained when using O + L datasets as complementary data to be used in a data fusion process. In addition, a new feature called "Greenhouse Detection Index" has been successfully developed and tested, yielding excellent results at the mapping phase. Finally, the semi-automatically extracted PCG land cover metrics, though depicting some variability, have reasonably reproduced the behaviour and temporal trend of the manually obtained ones (manual digitalization). These results can be translated to an exponential reduction of time and cost for analysing long-term PCG land cover change.

Keywords: Remote Sensing; Archival Aerial Orthoimages; Landsat data; Plastic Covered Greenhouses; Land Cover Change; Spatial Metrics

Nomenclature/Abbreviations

AREA_MN	Mean Patch Area [m^2]
BRI	Browning Reflectance Index
BSI	Bare Soil Index
ED2	Euclidean Distance 2
ENN_MN	Mean Euclidian Nearest Neighbour Distance [m]
ETM+	Enhanced Thematic Mapper Plus
F_β	Accuracy Measure [%]
FRAC_AM	Area Weighted Mean Patch Fractal Dimension
GDI	Greenhouse Detection Index
GSD	Ground Sample Distance
GT	Ground Truth
KIA	Kappa Index of Agreement
L	Landsat Images
MDI	Moment Distance Index
NDVI	Normalized Difference Vegetation Index
MRS	Multi-Resolution Segmentation
NP	Number of Patches [Greenhouses]
O	Orthoimages Aerial
OA	Overall Accuracy [%]
OBIA	Object-Based Image Analysis
O+L	Data Fusion (Orthoimage and Landsat data)
PA	Producer’s Accuracy [%]
PAN	Panchromatic Band
PCG	Plastic Covered Greenhouses
PD	Patch Density [nº/100 ha]
PGI	Plastic Greenhouse Index
PMLI	Plastic-Mulched Landcover Index
RF	Random Forest
SA	Study Area
SP	Scale Parameter
TM	Thematic Mapper
UA	User’s Accuracy [%]
VHR	Very High Resolution
Vi	Index Greenhouse Vegetable Land Extraction

1. INTRODUCTION

1.1. Contextualization

Greenhouses area around the world reached a value of 405,000 ha (FAO, 2013) throughout the first decade of the 21st century, mainly located in Europe (Mediterranean areas), North Africa, the Middle East and China. In the case of Spain, the surface dedicated to greenhouses has increased exponentially in the last decades from 546 ha in 1968 to 65,674 ha in 2016 (MAAMA, 2016). The largest concentration of greenhouses, mainly Plastic Covered Greenhouses (PCG), is located in the southeastern of Spain (southeastern Andalusia and Murcia). In 2016, Andalusia region presented up to 74% of the total greenhouse land cover in Spain (MAAMA, 2016). Focusing on the province of Almeria, where this study has been undertaken, the PCG area represents approximately 44% of the total area of greenhouses in Spain (CAPDR, 2016).

The predominant greenhouse in Almeria is the "Parral" type (the traditional Mediterranean greenhouse), typical of warm regions and characterized by its low height, plastic cover and wooden or aluminum structure (Valera Martínez, Belmonte Ureña, Molina Aiz, & López Martínez, 2014). From the landscape point of view, PCC areas are characterized by a set of very near patches constituting a continuous and shiny mosaic that has been called “Sea of plastic”, since there is no practically space between adjacent greenhouse patches (Fig. 1).

Overall, the arrival of this very intensive agricultural model to Almería led to a significant change in the patterns of land arrangement and landscape perception (Aznar-Sánchez & Sánchez-Picón, 2010). In fact, the aforementioned semi-industrialized agricultural model is linked to an important anthropic impact (Parra, Aguilar, & Calatrava, 2008) due to the construction of greenhouses and auxiliary infrastructure (e.g., road network, storage buildings, electrical network, irrigation network, irrigation ponds...). These activities contribute significantly to the modification of the environment (Arcidiacono & Porto, 2010). In this way, special care is required to carry out land planning and development tasks in these PCG areas, trying to minimize the environmental and visual impact (Rogge, Nevens, & Gulinck, 2008). To provide information on this issue, a panel of experts from the agri-food sector of the Community of Andalusia was consulted in a recent study. More than 50% of the panel members reported that, to date, there is practically no presence of the design component in the planning of agri-food facilities such as PCG areas (González-Yebra, Aguilar, & Aguilar, In press). Therefore, it seems clear that the study and monitoring of the design and planning of PCG areas is an aspect to be considered, mainly to avoid uncontrolled development leading to negative social and environmental consequences (Picuno, Tortora, & Capobianco, 2011; Tarantino & Figorito, 2012; Aguilar et al., 2014). According to Scarascia-Mugnozza, Sica and Picuno (2008) and Lanorte et al. (2017), the agricultural use of plastic sheet produces a problematic cycle associated with the generation of high volumes of waste in the rural areas. An interesting research line started in Spain in 1980's and 1990's, trying to link engineering and landscape architecture (García, Hernández, & Ayuga, 2003; Hernández, García, & Ayuga, 2004) through the study of the visual impact of rural buildings. However, new tools and methods are required in the particular case of PCG areas to facilitate a real approach to their land planning issue. In this context, the application of remote sensing technologies and information processing tools is a growing vector in the field of agricultural engineering (Alchanatis & Cohen, 2013) and precision agriculture (Mulla, 2013).

This work aims to propose, develop and evaluate a methodological procedure, constituting a valuable and efficient tool for the long-term analysis of PCG land cover change and spatial arrangement. To respond to this proposal, the following objectives are set:

1) Applying remote sensing techniques and freely access archival aerial orthoimages and satellite imagery to semi-automatically map PCG areas evolution through using an Object Based Image Analysis (OBIA).
2) Automatically determining some descriptive spatial metrics, extracted from previously classified objects (greenhouses), useful for carrying out landscape spatial analysis studies.

Figure 1. Left: Spatial arrangement of greenhouses in Almeria. Right: "Parral" greenhouse, the predominant greenhouse in Almería.

1.2. Background

1.2.1. Remote Sensing in PCG mapping

The methods for greenhouses automatic extraction from remote sensing is an important challenge for the scientific-technical community, due to the intrinsic characteristics of the design of these facilities (Agüera, Aguilar, & Aguilar, 2006; Agüera, Aguilar, & Aguilar, 2008; Tarantino & Figorito, 2012) and other related issues such as the spectral signature of plastic, season of the year, cleaning and conservation of the roof, greenhouse typology, etc.

The first works aimed at the detection of greenhouses using satellite data were carried out by using Landsat Thematic Mapper images (e.g., Mesev, Gorte, & Longley, 2000; Zhao, Li, Li, Yue, & Warner, 2004; Picuno et al., 2011). The main problem related to using Landsat images is their low geometric resolution. With the launch of the first very high resolution

(VHR) commercial optical satellites such as IKONOS and QuickBird in 1999 and 2001, respectively, the problem related to insufficient geometric resolution was properly solved.

Until a few years ago, most of the works on greenhouse detection had employed pixel-based classification techniques (Agüera et al., 2006; Agüera et al., 2008; Carvajal, Agüera, Aguilar, & Aguilar, 2010; Arcidiacono & Porto, 2011; Arcidiacono, Porto, & Cascone, 2012). However, during the last decade have emerged several works focused on land cover mapping from applying OBIA approaches, also comprising a wide range of sensors, features (spectral, textural, geometric, structural), classifiers and other variables of interest, showing the increasing interest about OBIA paradigm aroused among the scientific community (Ma et al., 2017). This trend can also be applied to the specific case of PCG mapping. To the best of our knowledge, the first work in which OBIA techniques were used to undertake greenhouses mapping from RGB aerial photography was published by Tarantino & Figorito (2012). After this work, other more recent studies have been contributed from using high resolution satellite images (Aguilar, Bianconi, Aguilar, & Fernández, 2014; Aguilar, Vallario, Aguilar, García Lorca, & Parente, 2015). Here it is necessary to highlight the pioneering work recently published by Aguilar, Nemmaoui, Novelli, Aguilar, & García Lorca (2016) where the combined use of high resolution image data and Landsat 8 time series was tested using an OBIA approach headed up to PCG mapping.

1.2.2. Spatial metrics application

In the last two decades, spatial metrics have emerged as a valuable tool to assess the territorial characteristics of ecological processes (Gustafson & Parker, 1994). They have been widely used as indicators for the study of spatial characteristics in urban landscapes (Geoghegan, Wainger, & Bockstael, 1997; Li, Yang, & Liu, 2008; Franco et al., 2005; Aguilera, Valenzuela-Montes, & Botequilha-Leitão, 2011). According to Herold, Goldstein,

& Clarke (2003), these metrics can be defined as a set of aggregate quantitative measures derived from the digital analysis of thematic maps (digital cartography). The information provided by these indicators is very valuable in relation to the evolution and changes undergone in a given landscape. This is the case of several investigations focused on combining Landsat imagery classification and landscape spatial metrics in urban environments. For example, Qu, Zhao, & Sun (2014) worked with remote sensing data and landscape metrics to explore spatio-temporal patterns of urbanization in two major cities in China, whereas Fenta et al. (2017) evaluated the dynamics and growth pattern in a city located in northern Ethiopia. Further information about the case of applying spatial metrics in the analysis of planning activities can be found in Botequilha-Leitão & Ahern (2002).

The aforementioned spatial metrics can be computed from Fragstats (McGarigal & Marks, 1995), a free software available since 1995 (current version 4.2) which works on raster image data. Fragstats contains an extensive library of metrics that can be calculated at class and/or landscape level, being currently the most used application in studies related to Landscape Ecology. However, there are other tools that work with raster digital data such as "LFT v2.0" (CLEAR, 2009), although it does not provide numerical values. It is widely known that raster format can present some limitations (depending on the final application), such as a high dependence on the pixel size in the results. This can be avoided by introducing the digital input information in vector format. In this sense, there are several tools that support vector format such as Patch Analyst (Rempel, Kaukinen, & Carr, 2012), PolyFrag (Maclean & Congalton, 2013) and IndiFrag (Sapena & Ruiz, 2015).

2. Study Sites

The two study areas are in the province of Almería (Southern Spain), just in the core of the greatest concentration of greenhouses in the world (Figure 2). The Study Area 1 (SA1) is located south-western Almería province (“Poniente” region). It comprises a rectangle area of about 2000 ha (4 km per 5 km) centred on the WGS84 geographic coordinates of 36°45'2.06"N and 2°42'20.77"W. The Study Area 2 (SA2) presents a rectangle area of 8000 ha (8 km per 10 km) centred on the WGS84 geographic coordinates of 36°53'44.04"N and 2°10'26.54"W. It is located south-eastern Almería province (“Levante” region). Since the concentration of greenhouses is much higher in the “Poniente” than in the “Levante” study site, different areas were selected for SA1 and SA2 in order to manage a similar number of greenhouses in both zones during the classification phase. Regarding territorial characterization, both zones are mainly used for intensive agricultural purposes, presenting an important dynamism due to the presence of a thriving agri-food industry based on greenhouse horticulture. Moreover, both study areas include urban zones which could hinder the automatic extraction of greenhouses due to their similar spectral response.

3. Dataset

The dataset of this work included archival aerial orthoimages (produced by the Spanish or Andalusia Governments) and Landsat imagery taken in 1984, 1999 and 2010. Both products are freely available through the Institute of Statistics and Cartography of Andalusia region (Spain) and the U.S Landsat archive, respectively.

The archival aerial orthoimages used in each study area and year were taken in September, 1984, September, 1999 and July, 2010. The orthoimages corresponding to 1985 were taken in B&W (i.e., one PAN band), presenting a geometric resolution of 1 m ground sample distance (GSD). Three bands RGB orthoimages with 1 m GSD were used in 1999, while RGB orthoimages with 0.5 m GSD were taken in 2010. It is important to note that their original geometric and radiometric (8 bits) resolutions, as well as the geolocation, were kept constant throughout the work.

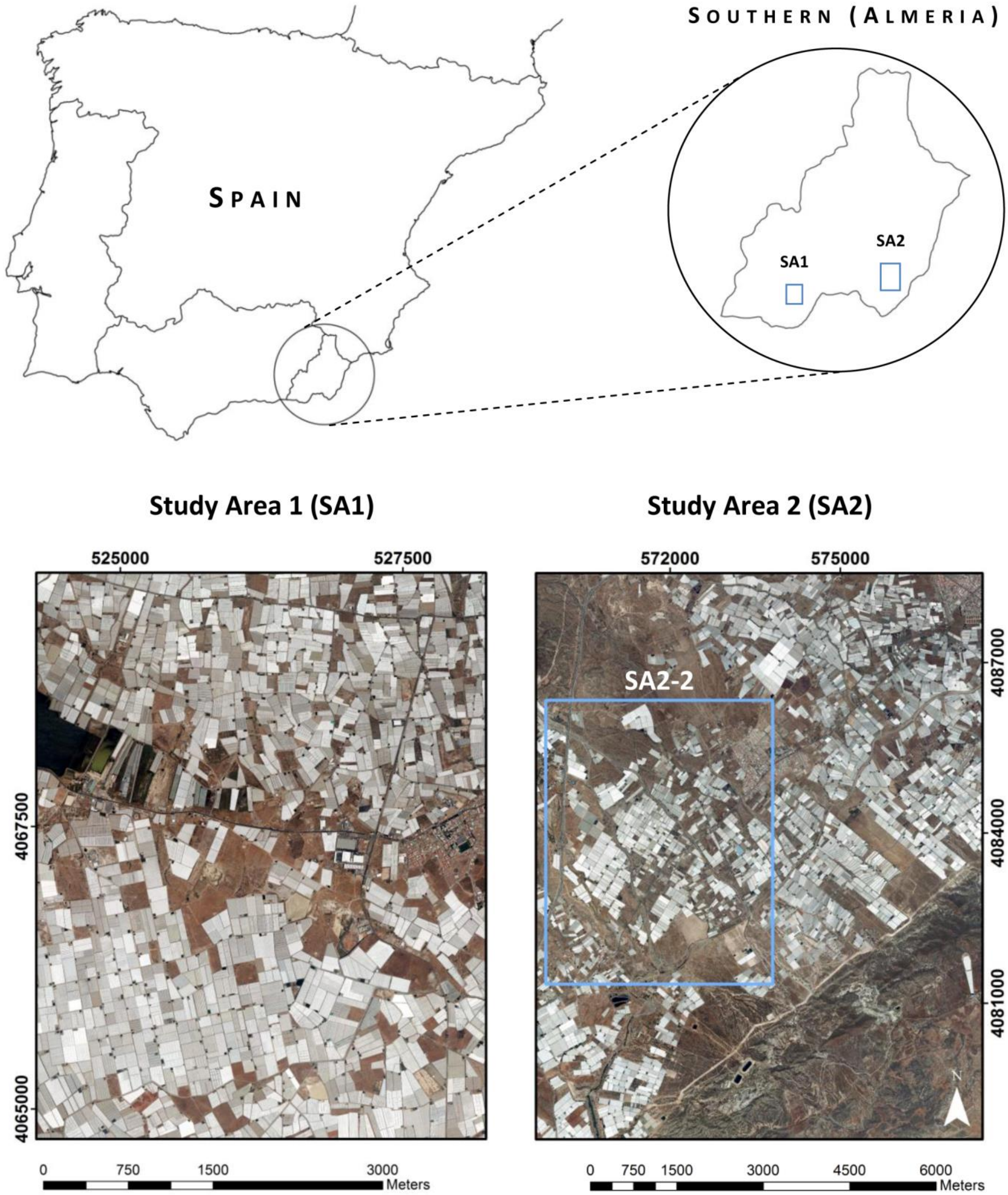

Figure 2. Location of the two study areas in Almería (Spain). Orthoimages taken in 2010. Coordinate system: ETRS89 UTM Zone 30N.

On the other hand, Landsat 5 Thematic Mapper (TM) multispectral images taken on October 14, 1984 (stage 1), and December 9, 2010 (stage 3), together with an image from Landsat 7 Enhanced Thematic Mapper Plus (ETM+) acquired on December 3, 1999 (stage 2), were used for the study area SA1. In the case of the study area SA2, the two used Landsat 5 images were taken on October 23, 1984 (stage 1), and November 16, 2010 (stage 3), whereas one Landsat 7 image was acquired on November 26, 1999 (stage 2). All Landsat images were downloaded as Level 1 Terrain Corrected (L1T) products. The temporal capture window ranged from October to December, just when PCG are not painted white (they have been whitewashed) to protect plants from excessive radiation and to reduce the heat inside the greenhouse (Aguilar et al., 2015). Six common MS bands with 30 m GSD from Landsat 5 TM and Landsat 7 ETM+ were analysed in this work: blue (B, 450–520 nm), green (G, 520–600 nm), red (R, 630–690 nm), near infrared (Nir, 765–900 nm), shortwave infrared-1 (Swir1, 1550–1700 nm) and shortwave infrared-2 (Swir2, 2085–2350 nm). The next processing step consisted of performing atmospheric correction by applying the ATCOR module, included in Geomatica v. 2016 (PCI Geomatics, Richmond Hill, ON, Canada), to the six Landsat multispectral images to attain ground reflectance values. It is worth noting that a proper co-registration between orthoimages and Landsat products was found.

4. Methodology

4.1. Object-based greenhouse mapping from remote sensing

4.1.1. Segmentation

The first step in the OBIA approach involves image segmentation to produce homogeneous and discrete objects. Later, these objects, rather than pixels, are used as the classification unit (Blaschke, 2010). In this work, high geometric resolution historical aerial orthoimages will be used to automatically obtain the segments corresponding to greenhouses in each study area (SA1 and SA2) and stage (1984, 1999 and 2010). For this task, we utilized the multi-resolution segmentation (MRS) algorithm implemented into the OBIA software eCognition v. 8.8 (Trimble, Sunnyvale, California, United States), an algorithm widely known and successfully employed under the context of remote sensing OBIA applications (Blaschke, 2010). This segmentation approach is a bottom-up region-merging technique starting with one-pixel objects or seeds. In numerous iterative steps, smaller objects are merged into larger ones (Baatz & Schäpe, 2000). The outcome of the MRS algorithm is controlled by three main factors: (1) scale parameter (SP), that determines the maximum allowed heterogeneity for the resulting segments; (2) the weight of colour and shape criteria in the segmentation process (Shape); and (3) the weight of the compactness and smoothness criteria (Compactness). In this way, thousands of segmentations from applying MRS algorithm were computed by means of a semi-automatic eCognition rule set characterized by a looping process varying the SP and Shape (from 0.1 to 0.9 with a step of 0.1) MRS tuning parameters. The Compactness parameter was fixed to 0.5 according to Liu & Xia (2010), Dragut, Csillik, Eisank, & Tiede (2014) or Kavzoglu & Yildiz (2014). In the context of the MRS algorithm, the users have to decide the bands combination and their corresponding weights to be applied in the segmentation process. In our case, the three RGB available bands were used in 1999 and 2010, while the PAN band was the only one used in 1984. Moreover, all the bands had the same weight in the MRS computation.

The selection of the best segmentation parameters is often a tedious trial-and-error process. To avoid this cumbersome task, a new free access command line tool named AssesSeg, developed by Novelli, Aguilar, Aguilar, Nemmaoui, & Tarantino (2017), was included in our proposal. AssesSeg implements a modified version of the Euclidean Distance 2 (ED2) supervised discrepancy measure proposed by Liu et al. (2012), which has been already successfully tested to estimate the best MRS segmentation parameters from Sentinel-

2, Landsat 8 and WorldView-2 imagery (Novelli, Aguilar, Nemmaoui, Aguilar, & Tarantino, 2016; Novelli et al., 2017). As a supervised segmentation quality metric, the modified ED2 works with a set of reference objects to evaluate segmentation goodness (Novelli et al., 2017). Thus, the lowest value of ED2 indicates the best segmentation. In this way, 100 polygons evenly distributed over the six orthoimages were manually digitized as reference greenhouses. Although in other works only 30 references had been used to compute ED2 (e.g., Liu et al., 2012; Witharana & Civco, 2014), Novelli et al. (2017) reported the importance of increasing the number of reference greenhouses to diminish the uncertainty in assessing the segmentation quality through the ED2 modified metric.

4.1.2. Features applied to OBIA classification

The features used to carry out the OBIA classification were extracted from both orthoimages and Landsat scenes by using eCognition v. 8.8. In the case of the orthoimages, object-based features such as mean values, standard deviation, shape index and brightness (only in coloured orthoimages) were used (further details about these features can be found in Trimble (2010)). Note that these object features were computed using three bands (RGB) in the case of the coloured orthoimages (8 features in total), while only one band (PAN) was employed from B&W orthoimages (3 features). Regarding Landsat 5 and 7 images, several spectral and vegetation indices depicted in Table 1 were computed from the six bands used. Most of these indices have already been tested for plastic cover detection such as Index Greenhouse Vegetable Land Extraction (Vi) (Zhao et al., 2004), Plastic-Mulched Landcover Index (PMLI) (Lu, Di, & Ye, 2014), Plastic Greenhouse Index (PGI) (Yang et al., 2017) and Moment Distance Index (MDI), originally proposed by Salas & Henebry (2012) and recently applied to greenhouse classification by Aguilar et al. (2016). Furthermore, a new index called Greenhouse Detection Index (GDI) has been proposed in this work (Table 1).

For the extraction of the aforementioned object-based features, the best segmentation attained for each study area and temporal stage (six cases) from using AssesSeg and the orthoimages was transferred to the correspondent Landsat image through the chessboard segmentation algorithm included in eCognition. In other words, object-based techniques were applied on Landsat 30 m GSD imagery but working on the orthoimage-based segmentation (from 0.5 m to 1 m GSD). It is important to highlight that the original 30 m GSD of the Landsat 5 and 7 images was increased to 1.875 m GSD by halving four times the original pixel size. This method to combine the segmentation produced by very high-resolution images with features extracted from medium resolution images using an OBIA approach has been already reported by Aguilar et al. (2015).

Table 1. Landsat indices tested in this work.

Abbrev.	**Tested Indices**	**Formulation**	**Reference**
NDVI	Normalized Difference Vegetation Index	$\frac{Nir-R}{Nir+R}$	(Rouse, Haas, Schell, & Deering, 1973)
BSI	Bare Soil Index	$\frac{(Swir1+R)-(Nir+B)}{(Swir1\ +R)+(Nir\ +B)}$	(Roy, Sharma, & Jain, 1996)
BRI	Browning Reflectance Index	$\frac{\left(\frac{1}{G}\right)-\left(\frac{1}{R}\right)}{Nir}$	(Merzlyak, Gitelson, Chivkunova, Solovchenko, & Pogosyan, 2003)
Vi	Index Greenhouse Vegetable Land Extraction	$\left(\frac{Swir1-Nir}{Swir1+Nir}\right)\times\left(\frac{Nir-R}{Nir+R}\right)$	(Zhao et al., 2004)
MDI	Moment Distance Index	$MD_{RP}-MD_{LP}$; For: $MD_{RP}=\sum_{i=\lambda RP}^{\lambda LP}\sqrt{\left(\rho_i^2+(\lambda RP-i)^2\right)}$ $MD_{LP}=\sum_{i=\lambda LP}^{\lambda RP}\sqrt{\left(\rho_i^2+(i-\lambda LP)^2\right)}$	(Salas & Henebry, 2012)
PMLI	Plastic-Mulched Landcover Index	$\frac{Swir1-R}{Swir1\ +R}$	(Lu et al., 2014)

PGI	Plastic Greenhouse Index	$100 \times \left(\frac{B \times (Nir - R)}{1 - \left(\frac{B + G + Nir}{3} \right)} \right)$	(Yang et al., 2017)
GDI	Greenhouse Detection Index	$\left(\frac{MDI}{3} \right) - \left(\frac{B - \left(\frac{Swir1 + Swir2}{2} \right)}{B + \left(\frac{Swir1 + Swir2}{2} \right)} \right)$	This study. University of Almería (UAL)

4.1.3. Random Forest classifier and classification accuracy assessment

Random Forest (RF) was selected to undertake the binary classification (Greenhouse and Others) of all the objects previously segmented for each study area and stage. RF is an ensemble, supervised and non-parametric classifier in which a majority vote over several bootstrapped decision trees is carried out. RF has performed good classification accuracies in several remote sensing studies (Breiman, 2001; Rodriguez-Galiano, Ghimire, Rogan, Chica-Olmo, & Rigol-Sanchez, 2012; Smith, 2010) and agricultural engineering applications (Gao et al., 2018; Khanchi, Birrell, & Mitchell, 2018), proving to be relatively robust to training size reduction and noise. Furthermore, RF can estimate the importance of features for the general classification of the land-cover categories and for the classification of each category (Rodriguez-Galiano et al., 2012). The reader can find further information on the mathematical formulation and the tuning parameters of RF classifier in Breiman (2001) and Dietterich (2000).

Six training sets, each one composed of 300 segments, were selected from the six best estimated segmentations (section 4.1.1) over each study area and temporal dataset. For each training set, one half of the objects were related to the “Greenhouse” class and the other half to the class labelled as “Other”. They were manually selected and considered as “pseudo-invariant” objects with similar geometry and same class for all the configurations tested. In a similar classification approach, Novelli et al. (2016) reported good results by using from 90 to 120 training objects. Approximately 2/3 of the available data were used to train the classifier and the remaining ones to estimate classifier accuracy. Then the selected RF classification was applied to the corresponding whole study area.

Three classification strategies were considered in this work: (i) using only the object-features extracted from the aerial orthoimage (O), (ii) using only the Landsat derived features (L), and, (iii) using all the available features from orthoimage and Landsat (O+L).

With regards to the accuracy assessment, six ground truths (GTs), consisting of shp format vector files, were manually digitized onto each of the orthoimages used in this work (Figures 4 and 5). These GTs were finally exported as raster files with 1 m pixel size. At this point, the classification results were compared with the corresponding GT by means of a pixel-based accuracy assessment to perform a real classification accuracy assessment. Confusion matrices were computed to provide a more reliable and complete accuracy indicator over the whole study areas (Aguilar et al., 2016). Note that if the accuracy assessment had been based on objects more than pixels, the error associated to the segmentation stage would not have been considered. The accuracy measures finally computed from the pixel-based confusion matrices were user's accuracy (UA), producer's accuracy (PA), overall accuracy (OA) and kappa coefficient (KIA) (Congalton, 1991). Finally, the F_β measure (Aksoy, Akcay, & Wassenaar, 2010; Longbotham et al, 2012), which provides a way of combining UA and PA into a single measure, was also computed according to the Equation (1), where the parameter β determines the weight given to the user's and producer's accuracies. The value used in this study (β = 1) weighs UA equal to PA.

$$F_\beta = \frac{(\beta^2 + 1)\times PA \times UA}{\beta^2 \times PA \times UA} \qquad (1)$$

4.2. Greenhouse landscape spatial metrics

The last stage of the proposed workflow consisted of a practical application headed up to analyse the PCG landscape fragmentation and spatial distribution. IndiFrag (Sapena & Ruiz,

2015) was the software tool used to compute some metrics related to landscape fragmentation from each classification data in vector format (Shapefile). Unlike other raster-based software tools, the vector data managed by IndiFrag allows working with topological relationships without losing the meaning of object or the relationship between contiguous objects of the same class. For the evaluation of the different inputs (vector files) provided by both OBIA classification strategies (i.e., O, L and O+L) and GTs, a set of metrics widely used in multitemporal landscape analysis have been selected. To facilitate later comparative analyses, the SA2 study area has been reduced to dimensions similar to SA1 within the context of this last stage, finally comprising a rectangle of 4 km by 5 km that can be observed in Figure 2 as "SA2 -2"(blue rectangle).

Table 2. Selected set of metrics for the evaluation of the input products. A_i = area of object i (m^2); n = total number of objects in the class; A_t = total area formed by all classes (m^2); P_i = perimeter of the object i (m); H_{ij} = distance from object i to nearest object j (from contour to contour) of the same class (m).

Abbrev.	**Tested Metric**	**Formulation**	**Reference**
AREA_MN	Mean Patch Area (m^2)	$\frac{\sum_{i=1}^{n} A_i}{n}$	Frenkel & Ashkenazi, 2008; Irwin & Bockstael, 2007; McGarigal, Cushman, & Ene, 2012
PD	Patch Density (nº/100 ha)	$\frac{n}{A_t} \times 10000 \times 100$	Herold, Scepan, & Clarke, 2002; Irwin & Bockstael, 2007; McGarigal et al., 2012; Gong, Yu, Joesting, & Chen, 2013
FRAC_AM	Area Weighted Mean Patch Fractal Dimension (dimensionless)	$\sum_{i=1}^{n} \left[\left(\frac{2 \times \ln(0{,}25 \times P_i)}{\ln(A_i)} \right) \times \left(\frac{A_i}{\sum_{i=1}^{n} A_i} \right) \right]$	Herold et al., 2002; McGarigal et al., 2012; Gong et al., 2013
ENN_MN	Mean Euclidian nearest neighbor distance (m)	$\frac{\sum_{i=1}^{n} (H_{ij})}{n}$	McGarigal et al., 2012; Gong et al., 2013

Since this work is focused on the spatial analysis of PCG landscape, the selected spatial metrics presented in Table 2 were calculated at class level (greenhouse class). The first step consisted of computing the Number of Patches "NP" or extracted greenhouses, a simple but essential measure for the purpose of this study because NP is needed to compute the rest of the metrics presented in Table 2. Note that the metrics listed in Table 2 are also provided by Fragstats, a raster-based software tool widely known and used in both scientific and technical publications in this field. In fact, the same Fragstats nomenclature has been followed in order to facilitate the reader's access to information, although the units and formulation are referred to those programmed in IndiFrag tool.

Some of the selected metrics have been already used in urban areas (Aguilera et al., 2011) to study processes of aggregation/fragmentation, elongation and dispersion. These metrics have been computed for the two study areas (SA1 and SA2), three years (1984, 1999 and 2010), and four methods tested in this work (GT, O, L and O+L), resulting in 24 study cases. Furthermore, the relative errors attained from the comparison of the metrics extracted from the GTs and their corresponding semi-automatic OBIA classification were taken as a direct estimate of the goodness of the remote sensing approach tested in this work.

5. Results and discussion

5.1. Segmentation stage

Table 3 presents the characteristics of the optimal segmentations attained from using MRS and AssesSeg over the six historical aerial orthoimages and considering that segmentation was focused on greenhouses. Although the minimum value of ED2 metric for each study area (SA1 and SA2) was obtained from B&W aerial orthoimage taken in 1984, all the six segmentations showed a very good visual correspondence with the individual greenhouses. In this way, the visual quality of a couple of ideal segmentations for SA1 and SA2 study areas can be seen in Figure 3.

It is important to highlight that the modified ED2 values computed in Table 3 were very similar to those reported in literature. For instance, Aguilar et al. (2018) reached a modified

ED2 value of 0.112 working on greenhouses by using 1.2 m GSD WorldView-3 MS orthoimages and 100 reference geometries. Slightly worse modified ED2 metric of 0.198 was achieved by Novelli et al. (2016) on the same greenhouse landscape working on 2 m GSD WorldView-2 MS orthoimage.

Table 3. Main parameters corresponding to optimal segmentation estimated from AssesSeg.

Area / Year	Minimum ED2	Scale	Shape	Compactness	Segmented Objects
SA1 / 1984	0.053	136	0.5	0.5	3143
SA2 / 1984	0.112	144	0.5	0.5	12621
SA1 / 1999	0.138	104	0.5	0.5	3125
SA2 / 1999	0.167	122	0.3	0.5	12059
SA1 / 2010	0.093	266	0.4	0.5	3060
SA2 / 2010	0.160	216	0.2	0.5	15436

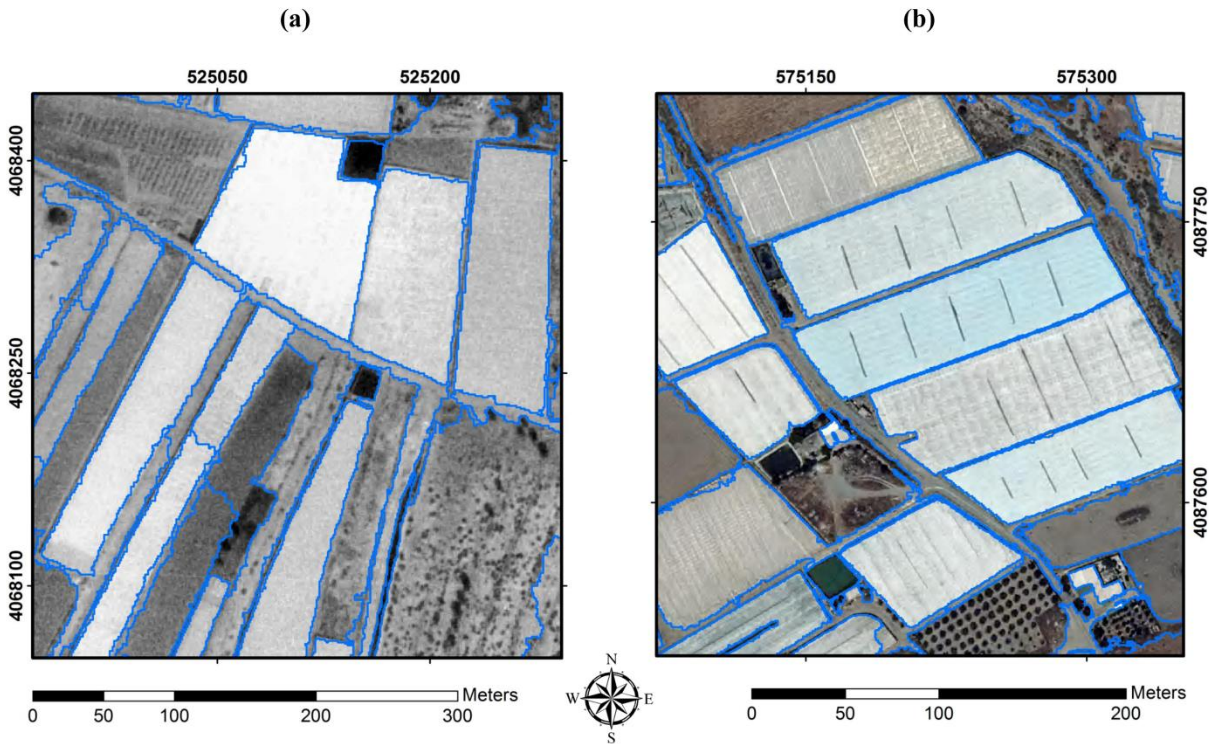

Figure 3. Visual quality of the segmentation results: (a) SA1, segmentation from B & W orthoimage taken in 1984, and (b) SA2, segmentation from coloured orthoimage taken in 2010.

The Scale parameter turned out to be very variable since it highly depends on the number of bands considered in MRS as well as the GSD of the input orthoimage. Regarding the

Shape parameter, it ranged from 0.5 to 0.2, which is consistent with the results reported by Aguilar et al. (2018). Finally, the ideal segmentations had a similar number of objects per area. At this point, it is important to remember that the SA1 study area was four times smaller than SA2.

5.2. OBIA classification stage

A summary of the results regarding the accuracy assessment is presented in Table 4. The best accuracy assessment results were achieved when the data fusion strategy O+L, involving both orthoimage and Landsat object features, was applied. In this case the values of OA were ranging from 92.05% (SA1 in 1999) to 98.58% (SA2 in 1984). Those results can be qualified as very good since the OA was always higher than 85%, which has been established as the minimum acceptable value for the classification results (Congalton & Green, 2008). Moreover, OA values of around 93% were reported by Aguilar et al. (2016) working on WorldView-2/3 and Landsat 8 optical images following a similar methodology. 90.25% OA was reported by Tarantino & Figorito (2012) working on digital true colour aerial data characterized by a GSD of 0.2 m, also following an OBIA approach. Celik & Koc-San (2018) achieved better OA (96.15%) by using RGB stereo aerial images with 0.3 m GSD, in this case also including a Digital Surface Model layer as complementary information to carry out the final classification.

Regarding the KIA values, the worst classification following the O+L strategy was yielded for SA2 in 1984 (KIA=0.79), precisely the dataset presenting the best OA. It is important to note that the percentage of area corresponding to the class “Others” resulted to be much higher in SA2 than in SA1. In this regards, bearing in mind that our target is focused on greenhouse mapping, the F_{β} measure for the class “Greenhouse” turned out to be the most valuable classification accuracy statistic. The F_{β} measures were ranging from 79.27% to

94.51%, values that do not differ from those achieved by Aguilar et al. (2014), who worked on mapping greenhouses from very high resolution satellite stereo pairs. The F_{β} statistic reached the worst values for both study areas in 1984. Note that in 1984 the aerial orthoimage only provided the PAN band with 1 m GSD. In fact, the visual discrimination between some greenhouses and other agricultural plots on these B&W orthoimages turned out to be very difficult, so likely incurring in some errors when accomplishing the manual digitizing for obtaining the GTs. The accuracy assessment based on the pixel-based confusion matrices showed that the most important contribution of adding Landsat object-based features to the orthoimage ones was just achieved in 1984. This positive contribution was decreasing when better orthoimages in terms of spectral and geometric quality were used (1999 and especially 2010). It is important to underline that the aerial orthoimage and Landsat scenes for each stage and study area were acquired at different dates (in some cases differing in several months), and the GTs were manually extracted from the orthoimages, which indicates that the Landsat classification might contain little mistakes.

Table 4. Pixel-based classification accuracy assessment for the class "Greenhouse" expressed as Overall Accuracy (OA), Kappa Index of Agreement (KIA) and F_{β} measure.

	Orthoimage			**Landsat**			**Ortho+Landsat**		
Area / Year	**OA (%)**	**KIA**	**F_{β} (%)**	**OA (%)**	**KIA**	**F_{β} (%)**	**OA (%)**	**KIA**	**F_{β} (%)**
SA1 / 1984	90.28	0.73	79.66	91.67	0.79	84.91	94.05	0.85	88.61
SA2 / 1984	97.33	0.58	59.33	97.36	0.68	69.31	98.58	0.79	79.27
SA1 / 1999	89.70	0.79	91.37	89.67	0.79	91.26	92.05	0.83	93.39
SA2 / 1999	93.96	0.78	81.24	92.21	0.77	81.45	96.31	0.87	89.44
SA1 / 2010	93.46	0.86	94.55	91.15	0.81	92.74	93.38	0.86	94.51
SA2 / 2010	94.07	0.84	87.67	93.42	0.83	87.84	95.83	0.89	91.41

Figures 4 and 5 show the manually digitized GTs and the OBIA classification results attained by using the best strategy (O+L) for SA1 and SA2, respectively. These figures depict the evolution over time of the PCG landscape in both study areas, allowing a visual quality assessment. The OBIA workflow proposed in this work yielded very good visual quality compared to the GTs in all the cases studied.

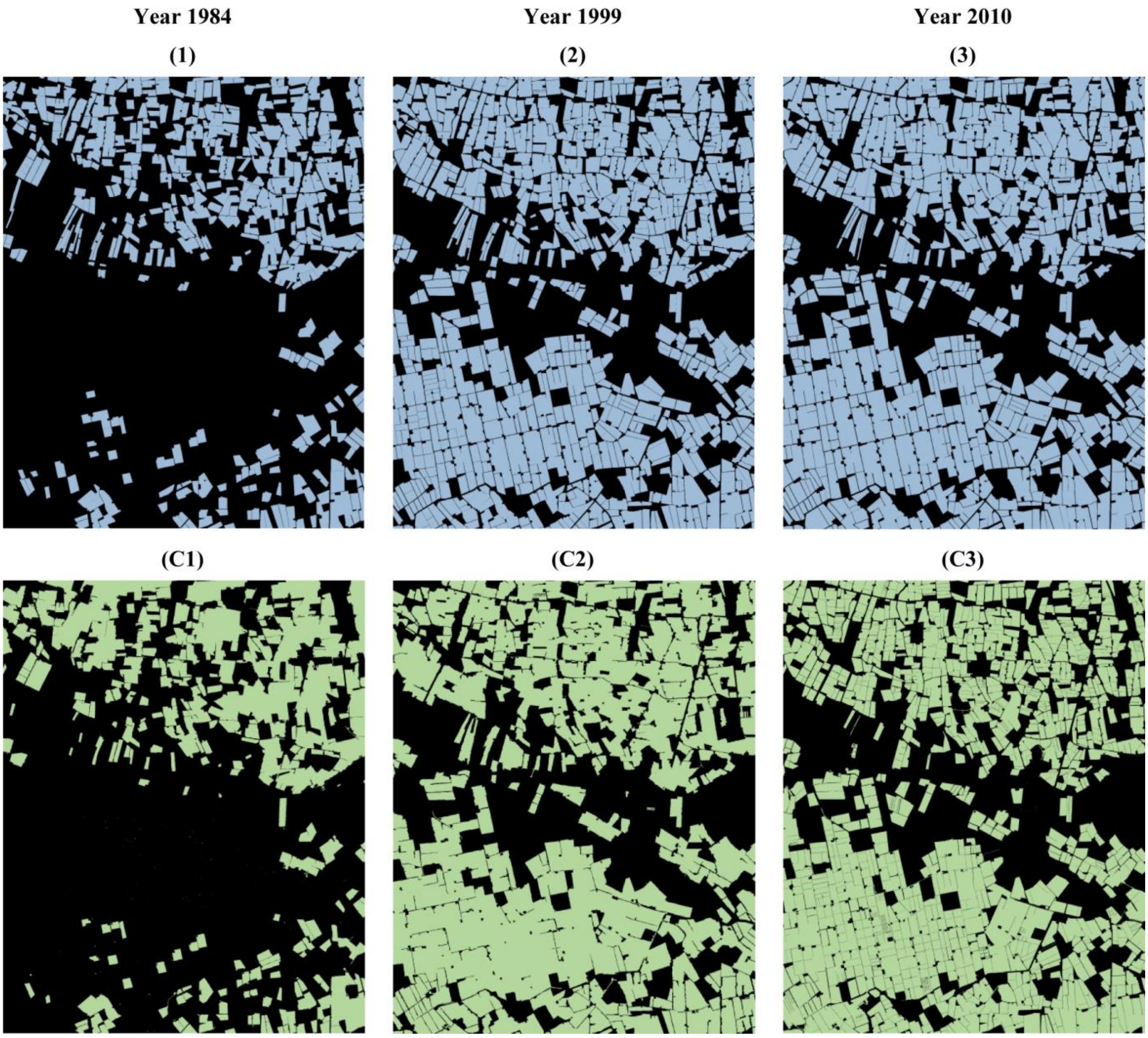

Figure 4. Visual classification quality for SA1 study area. First row, with greenhouses in blue color, shows the manually digitized ground truths for each stage (1) 1984, (2) 1999 and (3) 2010. Second row, with greenhouses in green color, depicts the OBIA classification from O+L strategy.

The relative importance for the classification of the main object-based features extracted from O+L strategy, according to RF classification and the Gini index, is depicted in Table 5. To the best knowledge of the authors, this is the first work comparing all the indices available in literature to detect PCG land cover by using remote sensing techniques.

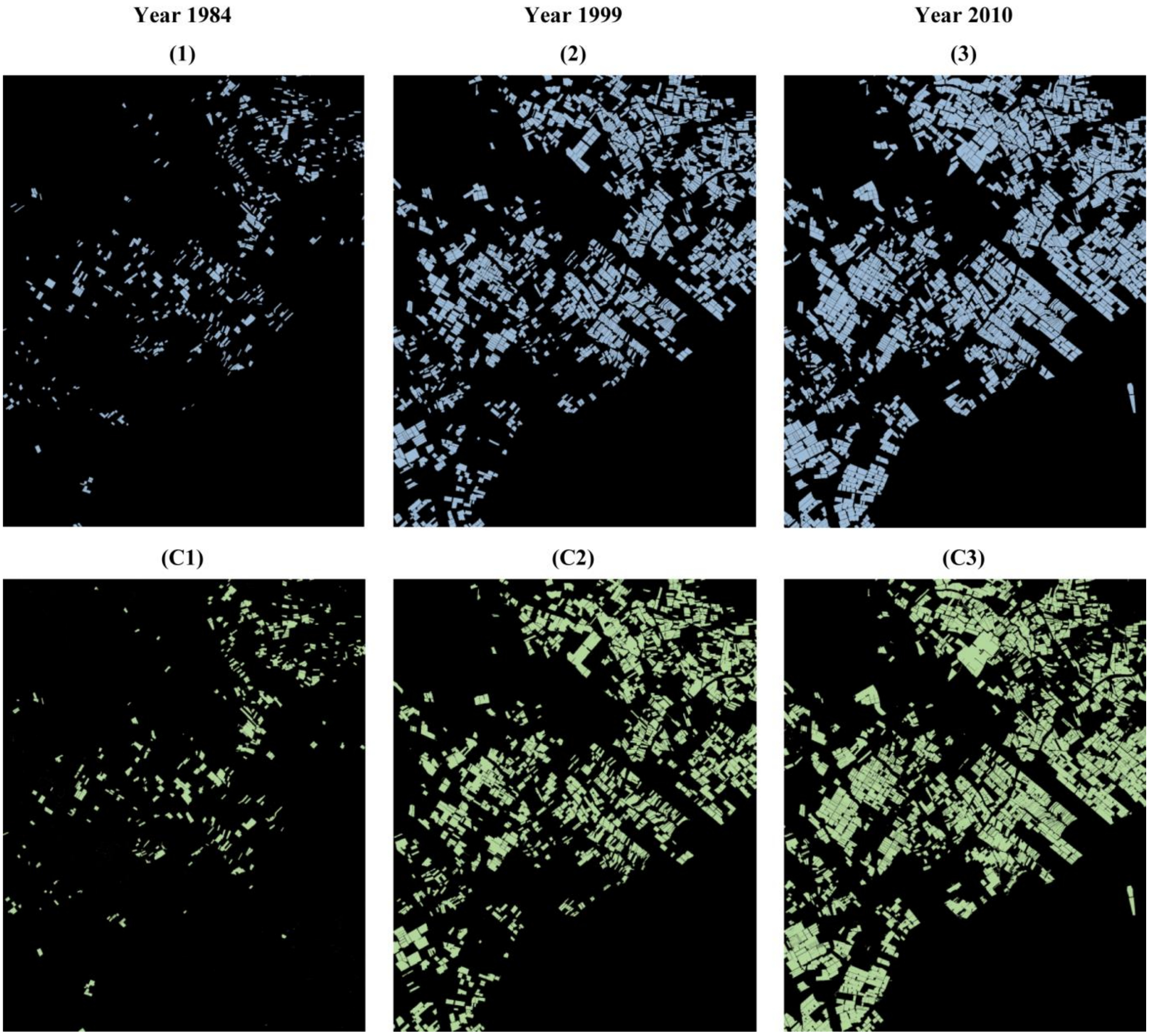

Figure 5. Visual classification quality for SA2 study area. First row, with greenhouses in blue color, shows the manually digitized ground truths for each stage (1) 1984, (2) 1999 and (3) 2010. Second row, with greenhouses in green color, shows the OBIA classification from O+L strategy .

The new index proposed in this work (GDI) was the feature ranked with the best score (94.2%) from considering all cases (relative mean importance of the three stages, Table 5). GDI was partially overcome by Brightness in 1999 and PMLI in 2010, anyway showing a relative importance higher than 92% in all cases. The inclusion of MDI index in the formulation of GDI can partially explain these remarkable results, since MDI has been successfully tested for PCG mapping working on Landsat 8 pansharpened images (Aguilar et al., 2016).

Table 5. Relative importance of the main object-based features used in O+L strategy provided by Random Forest procedure. For each studied stage (1984, 1999 and 2010), the mean values between the two study areas (SA1 and SA2) are depicted. The Brightness values of the images in B&W (1984) correspond exactly with the mean of its PAN band. All results are expressed in percentage.

Object-based Features	**Image Source**	**1984**	**1999**	**2010**	**Relative Mean Importance**
GDI	Landsat	95.5	95	92	94.2
Brightness	Orthoimage	79	97.5	92.5	89.7
PMLI	Landsat	80.5	80	94	84.8
MDI	Landsat	77.5	76	80	77.8
Vi	Landsat	74.5	77	77	76.2
Shape Index	Orthoimage	90	43	72.5	68.5
BSI	Landsat	67	61.5	65	64.5
PGI	Landsat	38	63	56.5	52.5
BRI	Landsat	54.5	37	47.5	46.3
NDVI	Landsat	32	33	38	34.3

Regarding the standard deviation feature derived from the aerial orthoimages, which may be considered as a first order texture feature, it presented an unstable behaviour, overall playing a minor role.

Finally, the shape index, a feature based on object geometry, took the highest importance in 1984, coinciding with the temporal dataset in which the spectral information, based on B&W images, would be qualified as poorer.

5.3. PCG landscape spatial metrics

Table 6 shows the results related to the selected spatial metrics provided by IndiFrag. Overall, the data fusion approach (O+L) extracted metrics presented the highest degree of similarity with the metrics computed from the GT. In the same way, the worst results were generally achieved from applying the L strategy. In the case of the data fusion approach (O+L) applied on the SA1 study area, relative errors below 10% were attained for all metrics except for EMM_MN. This trend was also maintained in the case of the SA2 study area, but here presenting more variable relative errors ranging from 3% to 22%. In general, a correlation was appreciated between the classification accuracy scores in the semi-automatically obtained vector maps (OBIA approach) and the goodness of their corresponding spatial metrics. This finding was also pointed out by Mas, Gao, & Navarrete Pacheco (2010) working on Landsat imagery classification.

Table 6. Different metrics to characterize PCG landscape fragmentation computed from different input products: Ground Truth (GT), aerial orthoimage classification strategy (O), Landsat classification strategy (L) and orthoimage plus Landsat data fusion classification strategy (O+L). Relative error, expressed in percentage with respect to the GT values, is presented in brackets, indicating overestimation/underestimation of the GT values by means of the positive/negative signs.

Input	**Area**	**Year**	**NP (Greenhouses)**	**AREA_MN (m^2)**	**PD (nº/100 ha)**	**FRAC_AM (dimensionless)**	**ENN_MN (m)**
GT		1984	919	5835	46.0	1.026	3.3
	SA1	1999	1461	8173	73.1	1.022	1.6
		2010	1540	7942	77.0	1.022	1.3
		1984	173	4860	8.7	1.026	41.1
	SA2	1999	730	5352	36.5	1.027	6.4
		2010	880	5891	44.0	1.025	4.5
O		1984	744 (-19)	5582 (-4)	37.2 (-19)	1.081 (5)	11.9 (266)
	SA1	1999	1349 (-8)	8805 (8)	67.5 (-8)	1.087 (6)	1.5 (-7)
		2010	1596 (4)	7357 (-7)	79.8 (4)	1.088 (6)	1.6 (19)
		1984	151 (-13)	3395 (-30)	7.6 (-13)	1.125 (10)	91.2 (122)
	SA2	1999	739 (1)	4366 (-18)	37.0 (1)	1.130 (10)	10.6 (67)
		2010	1139 (29)	4294 (-27)	57.0 (29)	1.149 (12)	6.2 (38)
L		1984	1026 (12)	5288 (-9)	51.3 (12)	1.132 (10)	2.6 (-21)
	SA1	1999	1557 (7)	7478 (-9)	77.9 (7)	1.102 (8)	0.6 (-62)
		2010	1719 (12)	7021 (-12)	86.0 (12)	1.103 (8)	0.7 (-49)
		1984	231 (34)	4550 (-6)	11.6 (34)	1.151 (12)	24.1 (-41)
	SA2	1999	1071 (47)	4335 (-19)	53.6 (47)	1.174 (14)	1.4 (-77)
		2010	1530 (74)	3730 (-37)	76.5 (74)	1.197 (17)	1.3 (-70)
O+L		1984	1002 (9)	5368 (-8)	50.1 (9)	1.122 (9)	3.7 (14)
	SA1	1999	1529 (5)	7896 (-3)	76.5 (5)	1.103 (8)	0.51 (-68)
		2010	1620 (5)	7313 (-8)	81.0 (5)	1.100 (8)	0.8 (-38)
		1984	167 (-3)	4317 (-11)	8.4 (-3)	1.141 (11)	32.7 (-20)
	SA2	1999	822 (13)	4519 (-16)	41.1 (-13)	1.150 (12)	3.9 (-38)
		2010	1053 (20)	4619 (-22)	52.7 (20)	1.147 (12)	3.3 (-26)

Figure 6 presents the results obtained from both the manually digitized maps (GT) and those semi-automatically extracted by OBIA classification using the O+L strategy. It can be observed that, although there were some mistakes, in the main, the fragmentation indices computed through remote sensing O+L strategy and GT had a very similar trend over time for the two study areas. To the best of our knowledge, this is the first time that these spatial metrics have been applied to PCG landscape, so there are no reference data in literature. Nonetheless, it has been demonstrated that spatial metrics or landscape indices are very sensitive to some aspects related to the remote sensing images analysis, especially geometric resolution (Wickham & Riiters 1995; Baldwin, Weaver, Schnekenburger, & Perera,2004).

Although good segmentations were obtained, they still presented some errors in greenhouse delineation (e.g., in many cases a greenhouse is segmented into several objects). These segmentation mistakes could explain some discrepancies found in the number of patches (NP), the density of objects (PD) and the average size (AREA_MN). In addition, the segmentation process produced zigzag edges on the polygon border as a result of the adaptation to the input raster orthoimages (Figure 3). This fact artificially increased the FRAC_AM metric, which provides information on the objects complexity, although the general trend of the FRAC_AM values were maintained over time. In the case of the EMM_MN metric, that gives a measure of the separation between adjacent objects belonging to the same class, it showed an important sensitivity to the misclassification of some objects as greenhouses. These classification errors, already reported by Aguilar et al. (2016), are usually found in the streets between two adjacent greenhouses (an example can be seen in Figure 1- Left).

The uncertainty associated with the analysis of satellite imagery data is extremely difficult to avoid. In this regards, Shao, Liu, & Zhao (2001) reported a great variation in the landscape metrics calculated from 23 maps with similar classification accuracy. However, it should be taken into account that the semi-automatic production of digital cartography from remote sensing techniques exponentially reduces exponentially the time and cost of production.

From the analysis of the metrics depicted in Table 6 and Figure 5, we can observe growth patterns similar to those provided in Aguilera et al. (2011) for urban areas. For example, NP, AREA_MN and PD metrics allowed characterizing the SA1 study area as an intensive agricultural zone with higher greenhouse density than the SA2 study site. In the same way, the FRAC_AM metric can be considered a compaction measure of the greenhouse shape, resulting very similar for both study areas. Finally, the dispersion of greenhouses, measured through ENN_MN metric, was much higher in SA2 than in SA1. In this way, spatial metrics were found to be very useful for the evaluation of PCG landscape analysis and planning.

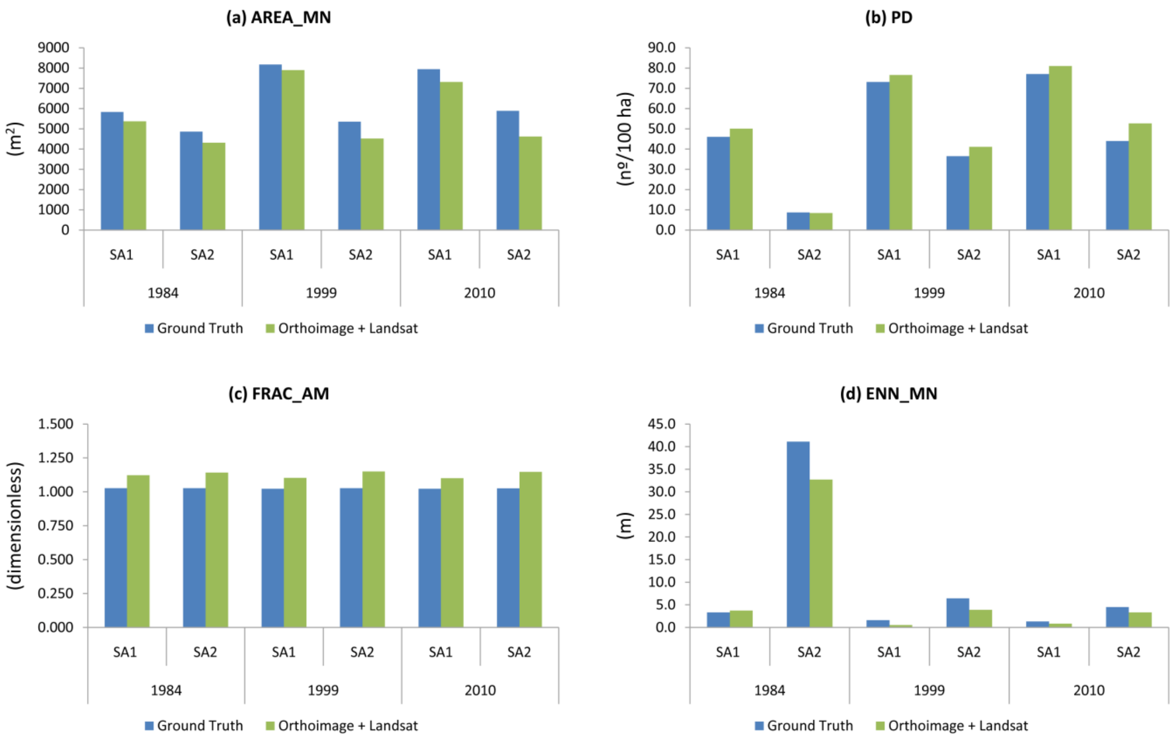

Figure 6. Comparison of the multitemporal evolution of some PCG landscape metrics obtained from manual digitizing (Ground Truth) and semiautomatic OBIA approach (Orthoimage+Landsat) for the two study areas.

The computed spatial metrics allow monitoring landscape changes and detecting growth patterns, what is extremely relevant for planners and decision makers. For example, in Figure 6 can be seen that the temporal evolution of the Levante region (SA2) shows a greater number of greenhouses (PD) with a higher average size (AREA_MN), together with a steady increment of PCG area over time, the latter revealed by the decrease in the average distance between neighbouring greenhouses (ENN_MN metric). This change in the PCG landscape is more sharpen between 1984 and 1999. According to the literature analysed, this scenario presents characteristics comparable to those typical of urbanization processes. A similar pattern occurs is detected in the western region (SA1), but this area has not undergone significant changes between 1999 and 2010 according to the low quantitative changes provided by the spatial metrics computed on the corresponding datasets.

6. Conclusions and Final Remarks

The findings obtained throughout this work allow concluding that the outlined semi-automatic OBIA approach based on remote sensing data fusion can be recommended for a timely and cost-effective way to carry out PCG landscape evolution studies where historical data are required. In fact, in terms of PCG mapping performance, the best results were obtained from using orthoimage and Landsat imagery datasets as complementary data to be entered in an OBIA data fusion process. This recommendation could be easily extended to other fields such as urban landscape and planning analysis.

Another novel contribution of this work has relied on the definition and validation of a new index for PCG mapping called Greenhouse Detection Index (GDI). GDI has demonstrated its valuable contribution to the OBIA classification process through applying Random Forest classifier, since it clearly exceeded the rest of the tested indices proposed in literature for detecting PCG land cover. Further research has to be made in order to check GDI performance on other remote sensing data sources (e.g., WorldView-3 or Sentinel-2 satellite imagery).

The semi-automatically extracted PCG landscape metrics, though depicting some variability, have reasonably reproduced the behaviour and temporal trend of the manually obtained ones (manual digitizing). At this point, it is necessary to take into account the inherent limitations of this study. In fact, as a pioneering work devoted to semi-automatically extracting PCG landscape spatial metrics, we strongly recommend testing and exploring the behaviour of other different spatial metrics which could also contribute excellent results for PCG landscape analysis and planning. These results could be translated to an exponential reduction of time and cost for carrying out this kind of landscape analysis studies without losing their required accuracy.

In summary, the approach devised and tested in this work can provide a very valuable tool for landscape designers and planners, thus contributing to the sustainable development of these very intensive agricultural models.

Acknowledgements

This work has been supported and financed by an FPI predoctoral fellowship (first author) granted in the framework of University of Almeria Research Programme. Additionally, this work has received financial support from the "GreenhouseSat" research project (Grant Reference AGL2014-56017-R) funded by the Spanish Ministry of Economy and Competitiveness (Spain) and the European Regional Development Fund (European Union) partially finances the research project GreenhouseSat (AGL2014-56017-R). This work takes part of the general research lines promoted by the Agrifood Campus of International Excellence ceiA3, Spain (http://www.ceia3.es/en).

References

Agüera, F., Aguilar, M.A., & Aguilar, F.J. (2006). Detecting greenhouse changes from QB imagery on the Mediterranean Coast. *International Journal of Remote Sensing*, 27(21), 4751-4767. doi:10.1080/01431160600702681

Agüera, F., Aguilar, F.J., & Aguilar, M.A. (2008). Using texture analysis to improve per-pixel classification of very high resolution images for mapping plastic greenhouses. *ISPRS Journal of Photogrammetry and Remote Sensing*, 63(2008), 635-646. doi:10.1016/j.isprsjprs.2008.03.003

Aguilar, M.A., Bianconi, F., Aguilar, F.J., & Fernández, I. (2014). Object-based greenhouse classification from GeoEye-1 and WorldView-2 stereo imagery. *Remote Sensing*, 6, 3554-3582. doi:10.3390/rs6053554

Aguilar, M.A., Vallario, A., Aguilar, F.J., García Lorca, A., & Parente, C. (2015). Object-Based Greenhouse Horticultural Crop Identification from Multi-Temporal Satellite Imagery: A Case Study in Almeria, Spain. *Remote Sensing*, 7, 7378-7401. doi:10.3390/rs70607378

Aguilar, M.A., Nemmaoui, A., Novelli, A., Aguilar, F.J., & García Lorca, A. (2016). Object-Based Greenhouse Mapping Using Very High Resolution Satellite Data and Landsat 8 Time Series. *Remote Sensing*, 8, 513. doi:10.3390/rs8060513

Aguilar, M.A., Novelli, A., Nemamoui, A., Aguilar, F.J., García Lorca, A., & González-Yebra, O. (2018). Optimizing Multiresolution Segmentation for Extracting Plastic Greenhouses from WorldView-3 Imagery. In G. De Pietro, L. Gallo, R. J. Howlett, L. C. Jain (Eds.), *Smart Innovation, Systems and Technologies* (pp. 31-40). Springer International Publishing AG, Cham, Switzerland.

Aguilera, F., Valenzuela-Montes, L.M., & Botequilha-Leitão, A. (2011). Landscape metrics in the analysis of urban land use patterns: a case study in a Spanish metropolitan area. *Landscape and Urban Planning*, 99(3-4), 226-238. doi:10.1016/j.landurbplan.2010.10.004

Aksoy, S., Akcay, H.G., & Wassenaar, T. (2010). Automatic mapping of linear woody vegetation features in agricultural landscapes using very high-resolution imagery. *IEEE Transactions on Geoscience and Remote Sensing*, 48, 511-522. doi:10.1109/TGRS.2009.2027702

Alchanatis, V., & Cohen, Y. (2013). Special issue on sensors in agriculture. *Biosystems Engineering.* 114(4), 357. doi: 10.1016/j.biosystemseng.2013.01.007

Arcidiacono, C., & Porto, S.M.C. (2010). A model to manage crop-shelter spatial development by multi-temporal coverage analysis and spatial indicators. *Biosystems Engineering*, 107(2), 107-122. doi:10.1016/j.biosystemseng.2010.07.007

Arcidiacono, C., & Porto, S.M.C. (2011). Improving per-pixel classification of crop-shelter coverage by texture analyses of high-resolution satellite panchromatic images. *Journal of Agricultural Engineering*, 42(4), 9-16. doi.org/10.4081/jae.2011.4.9

Arcidiacono, C., Porto, S.M.C., & Cascone, G. (2012). Accuracy of crop-shelter thematic maps: A case study of maps obtained by spectral and textural classification of high-resolution satellite images. *Journal of Food Agriculture and Environment*, 10, 1071-1074.

Aznar-Sánchez, J.A., & Sánchez-Picón, A. (2010). Innovación y distrito en torno a un "milagro": la configuración del sistema productivo local de la agricultura intensiva de Almería (Innovation and district around a "miracle": The configuration of the local productive system of intensive agriculture in Almería). *Revista de Historia Industrial*, 42(1), 157-193 (in Spanish: English abstract).

Baatz, M., & Schäpe, M. (2000). Multiresolution segmentation - An optimization approach for high quality multi-scale image segmentation. In J. Strobl, T. Blaschke, G. Griesebner (Eds.), *Angewandte Geographische Informations-Verarbeitung XII*. (pp. 12-23). Wichmann Verlag, Karlsruhe.

Baldwin, D.J.B., Weaver, K., Schnekenburger, F., & Perera, A.H. (2004). Sensitivity of landscape pattern indices to input data characteristics on real landscapes: implications for their use in natural disturbance emulation. *Landscape Ecology*, 19(3), 255-271. doi.:10.1023/B:LAND.0000030442.96122.ef

Blaschke, T. (2010). Object based image analysis for remote sensing. *ISPRS journal of photogrammetry and remote sensing*, 65, 2-16. doi.:10.1016/j.isprsjprs.2009.06.004

Botequilha-Leitão, A., & Ahern, J. (2002). Applying landscape concepts and metrics in sustainable landscape planning. *Landscape and Urban Planning*, 59, 65-93. doi.:10.1016/S0169-2046(02)00005-1

Breiman, L. (2001). Random Forests. *Machine Learning*, 45, 5-32. doi.:10.1023/A:1010933404324

CAPDR (2016). *Cartografía de invernaderos en el litoral de Andalucía Oriental (Cartography of greenhouses on the coast of Eastern Andalusia)*. Consejería de Agricultura, Pesca y Desarrollo Rural, Andalucía (in Spanish).

Carvajal, F., Agüera, F., Aguilar, F.J., & Aguilar, M.A. (2010). Relationship between atmospheric correction and training site strategy with respect to accuracy of greenhouse detection process from very high resolution imagery. *International Journal of Remote Sensing*, 31(11), 2977-2994. doi.:10.1080/01431160902946580

Celik, S., & Koc-San, D. (2018). Greenhouse Detection Using Aerial Orthophoto and Digital Surface Model. In G. De Pietro, L. Gallo, R. J. Howlett, L. C. Jain (Eds.), *Smart Innovation, Systems and Technologies* (pp. 51-59). Springer International Publishing AG, Cham, Switzerland.

CLEAR (2009). Center for Land Use Education and Research. Landscape Fragmentation Tool (LFT v2.0). Retrieved from: https://goo.gl/dyvpZZ

Congalton, R.G. (1991). A Review of Assessing the Accuracy of Classifications of Remotely Sensed Data. *Remote Sensing of Environment*, 37, 35-46. doi:10.1016/0034-4257(91)90048-B

Congalton, R.G., & Green, K. (2008). *Assessing the Accuracy of Remotely Sensed Data: Principles and Practices*. CRC Press.

Dietterich, T.G. (2000). An experimental comparison of three methods for constructing ensembles of decision trees: bagging, boosting, and randomization. *Machine Learning*, 40, 139-157. doi:10.1023/A:1007607513941.

Dragut, L., Csillik, O., Eisank, C., & Tiede, D. (2014). Automated parameterisation for multi-scale image segmentation on multiple layers. *ISPRS Journal Photogrammetry and Remote Sensing*, 88, 119-127. doi:10.1016/j.isprsjprs.2013.11.018

FAO (2013). *Good Agricultural Practices for Greenhouse Vegetable. Crops. Principles for Mediterranean Climate Areas*. Food and Agriculture Organization of the United Nations, Rome.

Fenta, A. A., Yasuda, H., Haregeweyn, N., Belay, A. S., Hadush, Z., Gebremedhin, M. A., & Mekonnen, G. (2017). The dynamics of urban expansion and land use/land cover changes using remote sensing and spatial metrics: the case of Mekelle City of northern Ethiopia. *International Journal of Remote Sensing*, 38(14), 4107-4129. doi:10.1080/01431161.2017.1317936

Franco, D., Bombonato, A., Mannino, I., Ghetti, P.F., & Zanetto, G. (2005). The evaluation of a planning tool through the landscape ecology concepts and methods. *Management of Environmental Quality*: *An International Journal*, 16(1), 55-70. doi:10.1108/14777830510574344

Frenkel, A., & Ashkenazi, M. (2008). Measuring urban sprawl: How can we deal with it?. *Environment and Planning B: Urban Analytics and City Science*, 35(1), 56-79. doi:10.1068/b32155

Gao, J., Nuyttens, D., Lootens, P., He, J., & Pieters, J.G. (2018). Recognising weeds in a maize crop using a random forest machine-learning algorithm and near-infrared snapshot mosaic hyperspectral imagery. *Biosystems Engineering*, 170, 39-50. doi: 10.1016/j.biosystemseng.2018.03.006

García, L., Hernández, J., & Ayuga, F. (2003). Analysis of the exterior colour of agroindustrial buildings: a computer arded approach to landscape integration. *Journal of Environmental Management*, 69(1), 93-104. doi:10.1016/S0301-4797(03)00121-X

Geoghegan, J., Wainger, L.A., & Bockstael, N.E. (1997). Spatial landscape indices in a hedonic framework: an ecological economics analysis using GIS. *Ecological Economics*. 23(3), 251-264.

Gong, C., Yu, S., Joesting, H., & Chen, J. (2013). Determining socioeconomic drivers of urban forest fragmentation with historical remote sensing images. *Landscape and Urban Planning*. 117, 57-65. doi:10.1016/j.landurbplan.2013.04.009

González-Yebra, O., Aguilar M.A., & Aguilar F.J. (In Press, 2017). A first approach to the Design Component in the Agri-food Industry of Southern Spain. *Revista de la Facultad de Ciencias Agrarias UNCuyo*.

Gustafson, E. J., & Parker, G.R. (1994). Using an index of habitat patch proximity for landscape design. *Landscape and Urban Planning*, 29(2-3), 117-130. doi:10.1016/0169-2046(94)90022-1

Hernández, J., García, L., & Ayuga, F. (2004). Integration Methodologies for Visual Impact Assessment of Rural Buildings by Geographic Information Systems. *Biosystems Engineering*, 88(2), 255-263. doi:10.1016/j.biosystemseng.2004.02.008

Herold, M., Scepan, J., & Clarke, K.C. (2002). The use of remote sensing and landscape metrics to describe structures and changes in urban land uses. *Environment and Planning A: Economy and Space*, 34(8), 1443-1458. doi:10.1068/a3496

Herold, M., Goldstein, N.C., & Clarke, K.C. (2003). The spatiotemporal form of urban growth: measurement, analysis and modeling. *Remote Sensing of Environment*, 86, 286-302. doi:10.1016/S0034-4257(03)00075-0

Irwin, E.G., & Bockstael, N.E. (2007). The evolution of urban sprawl: evidence of spatial heterogeneity and increasing land fragmentation. *Proceedings of the National Academy of Sciences*, 104(52), 20672-20677. doi:10.1073/pnas.0705527105

Kavzoglu, T., & Yildiz, M. (2014). Parameter-Based Performance Analysis of Object-Based Image Analysis Using Aerial and QuikBird-2 Images. *ISPRS Annals of Photogrammetry, Remote Sensing and Spatial Information Sciences*, II-7, 31-37. doi: 10.5194/isprsannals-II-7-31-2014

Khanchi, A., Birrell, S., & Mitchell, R.B. (2018). Modelling the influence of crop density and weather conditions on field drying characteristics of switchgrass and maize stover using random forest. *Biosystems Engineering*, 169, 71-84. doi: 10.1016/j.biosystemseng.2018.02.002

Lanorte A., De Santis F., Nolè G., Blanco I., Loisi R. V., Schettini E., & Vox G. (2017). Agricultural plastic waste spatial estimation by Landsat 8 satellite images. *Computers and Electronics in Agriculture*, 141, 35-45. doi: 10.1016/j.compag.2017.07.003

Li, X., Yang, Q., & Liu, X. (2008). Discovering and evaluating urban signatures for simulating compact development using cellular automata. *Landscape and Urban Planning*. 86, 177-186. doi:10.1016/j.landurbplan.2008.02.005

Liu, D., & Xia, F. (2010). Assessing object-based classification: Advantages and limitations. *Remote Sensing Letters*, 1(4), 187-194. doi:10.1080/01431161003743173

Liu, Y., Biana, L., Menga, Y., Wanga, H., Zhanga, S., Yanga, Y., Shaoa, X., & Wang, B. (2012). Discrepancy measures for selecting optimal combination of parameter values in object based image analysis. *ISPRS Journal Photogrammetry and Remote Sensing*, 68, 144-156.

Longbotham, N., Chaapel, C., Bleiler, L., Padwick, C., Emery, W.J., & Pacifici, F. (2012). Very high resolution multiangle urban classification analysis. *IEEE Transactions on Geoscience and Remote Sensing*, 50(4), 1155-1170. doi: 10.1109/TGRS.2011.2165548

Lu, L., Di, L., & Ye, Y. (2014). A Decision-tree classifier for extracting transparentplastic-mulched landcover from Landsat-5 TM images. *IEEE Journal of Selected Topics in Applied Earth Observations and Remote Sensing*. 7(11), 4548-4558. doi:10.1109/JSTARS.2014.2327226

Ma, L., Li, M., Ma, X., Cheng, L., Du, P., & Liu, Y. (2017). A review of supervised object-based land-cover image classification. *ISPRS Journal of Photogrammetry and Remote Sensing*, 130, 277-293. doi:10.1016/j.isprsjprs.2017.06.001

MAAMA (2016). *Encuesta sobre superficies y rendimientos de cultivos en España (ESYRCE) (Survey on areas and crop yields in Spain)*. Ministerio de Agricultura, Alimentación y Medio Ambiente, Madrid (in Spanish).

Maclean, M.G., & Congalton, R.G. (2013). PolyFrag: a vector-based program for computing landscape metrics. *GIScience & Remote Sensing*, 50(6), 591-603. doi:10.1080/15481603.2013.856537

Mas, J.F., Gao, Y., & Navarrete Pacheco, J.A. (2010). Sensitivity of landscape pattern metrics to classification approaches. *Forest Ecology and Management*, 259(7), 1215-1224. doi:10.1016/j.foreco.2009.12.016

McGarigal, K., & Marks, B. J. (1995). *FRAGSTATS: Spatial pattern analysis program for Quantifying Landscape Structure*. General Technical Report PNW-GTR-351. Department of Agriculture, United States.

McGarigal, K., Cushman, S., & Ene, E. (2012). FRAGSTATS v4: Spatial Pattern Analysis Program for Categorical and Continuous Maps. Retrieved from: https://goo.gl/P4Mqg8

Merzlyak, M. N., Gitelson, A. A., Chivkunova, O. B., Solovchenko, A. E., & Pogosyan, S. I. (2003). Application of Reflectance Spectroscopy for Analysis of Higher Plant Pigments. *Russian Journal of Plant Physiology*, 50(5), 704-710. Translated from Fiziologiya Rastenii, 50(5), 785-792.

Mesev, V., Gorte, B., & Longley, P.A. (2000). Modified Maximum-Likelihood Classification Algorithms and Their Application to Urban Remote Sensing. In J.-P. Donnay, M.J. Barnsley, P.A. Longley (Eds), *Remote Sensing and Urban Analysis* (pp. 62-83). Taylor & Francis, New York, USA.

Mulla, D.J. (2013). Twenty five years of remote sensing in precision agriculture: Key advances and remaining knowledge gaps. *Biosystems Engineering*, 114(4), 358-371. doi: 10.1016/j.biosystemseng.2012.08.009

Novelli, A., Aguilar, M.A., Nemmaoui, A., Aguilar, F.J., & Tarantino, E. (2016). Performance evaluation of object based greenhouse detection from Sentinel-2 MSI and Landsat 8 OLI data: A case study from Almería (Spain). *International Journal of Applied Earth Observation and Geoinformation*. 52, 403-411. doi:10.1016/j.jag.2016.07.011

Novelli, A., Aguilar, M.A., Aguilar, F.J., Nemmaoui, A., & Tarantino, E. (2017). AssesSeg-A Command Line Tool to Quantify Image Segmentation Quality: A Test Carried Out in Southern Spain from Satellite Imagery. *Remote Sensing*. 9(1), 40. doi:10.3390/rs9010040

Parra, S., Aguilar, F.J., & Calatrava, J. (2008). Decision modelling for environmental protection: the contingent valuation method applied to greenhouse waste management. *Biosystems Engineering*, 99(4), 469-477. doi:10.1016/j.biosystemseng.2007.11.016

Picuno, P., Tortora, A., & Capobianco, R. L. (2011). Analysis of plasticulture landscapes in Southern Italy through remote sensing and solid modelling techniques. *Landscape and Urban Planning*, 100 (1-2), 45-56. doi:10.1016/j.landurbplan.2010.11.008

Qu, W., Zhao, S., & Sun, Y. (2014). Spatiotemporal patterns of urbanization over the past three decades: a comparison between two large cities in Southwest China. *Urban Ecosystems*, 17(3), 723-739. doi:10.1007/s11252-014-0354-3

Rempel, R.S., Kaukinen, D., & Carr, A.P. (2012). Patch Analyst and Patch Grid. Ontario Ministry of Natural Resources, Centre for Northern Forest Ecosystem Research, Thunder Bay. Retrieved from: https://goo.gl/H8ylR

Rodriguez-Galiano, V.F., Ghimire, B., Rogan, J., Chica-Olmo, M., & Rigol-Sanchez, J.P. (2012). An assessment of the effectiveness of a random forest classifier forland-cover classification. *ISPRS Journal of Photogrammetry and Remote Sensing*, 67, 93-104. doi:10.1016/j.isprsjprs.2011.11.002

Rogge, E., Nevens, F., & Gulinck, H. (2008). Reducing the visual impact of ‘greenhouse parks’ in rural landscapes. *Landscape and Urban Planning*, 87(1), 76-83. doi:10.1016/j.landurbplan.2008.04.008

Rouse, J.W., Haas, R.H., Schell, J.A., & Deering, D.W. (1973). Monitoring vegetation systems in the great plains with ERTS. In Proceedings of the Third ERTS Symposium, *NASA SP-351*, (pp. 309-317). NASA, United States.

Roy, P.S., Sharma, K.P., & Jain, A. (1996). Stratification of density in dry deciduous forest using satellite remote sensing digital data —An approach based on spectral indices. *Journal of Biosciences*, 21(5), 723-734. doi:10.1007/BF02703148

Salas, E.A.L., & Henebry, G.M. (2012). Separability of maize and soybean in the spectral regions of chlorophyll and carotenoids using the moment distance index. *Israel Journal of Plant Sciences*, 60(1-2), 65-76. doi:10.1560/IJPS.60.1-2.65

Sapena, M., & Ruiz, L.A. (2015). Descripción y cálculo de índices de fragmentación urbana: Herramienta *IndiFrag* (Description and extraction of urban fragmentation indices: The *IndiFrag* tool). *Revista de Teledetección*, 43, 77-90 (in Spanish: English abstract). doi: 10.4995/raet.2015.3476

Scarascia-Mugnozza G., Sica C., & Picuno P. (2008). The Optimization of the Management of Agricultural Plastic Waste in Italy Using a Geographical Information System. *Acta Horticulturae*, 801, 219-226. doi: 10.17660/ActaHortic.2008.801.20

Shao, G., Liu, D., & Zhao, G. (2001). Relationships of image classification accuracy and variation of landscape statistics. *Canadian Journal of Remote Sensing*, 27, 33-43. doi:10.1080/07038992.2001.10854917

Smith, A. (2010). Image segmentation scale parameter optimization and land cover classification using the random forest algorithm. *Journal of Spatial Science*, 55, 69-79. doi:10.1080/14498596.2010.487851

Tarantino, E., & Figorito, B. (2012). Mapping Rural Areas with Widespread Plastic Covered Vineyards Using True Color Aerial Data. *Remote Sensing*, 4(7), 1913-1928. doi:10.3390/rs4071913

Trimble (2010). *eCognition® Developer 8.64.0 Reference Book*. Munich, Germany - Trimble Germany GmbH.

Valera Martínez, D. L., Belmonte Ureña, L. J., Molina Aiz, F. D., & López Martínez, A. (2014): *Los invernaderos de Almería. Análisis de su tecnología y rentabilidad (The greenhouses of Almería. Analysis of its technology and profitability)*. Colección Serie Economía, Cajamar Caja Rural, Almería (in Spanish).

Wickham, J.D., & Riitters, K.H. (1995). Sensitivity of landscape metrics to pixel size. *International Journal of Remote Sensing*, 16(18), 3585-3594. doi:10.1080/01431169508954647

Witharana, C., & Civco, D.L. (2014). Optimizing multi-resolution segmentation scale using empirical methods: Exploring the sensitivity of the supervised discrepancy measure Euclidean Distance 2 (ED2). *ISPRS Journal of Photogrammetry and Remote Sensing*, 87, 108-121. doi:10.1016/j.isprsjprs.2013.11.006

Yang, D., Chen, J., Zhou, Y., Chen, X., Chen, X., & Cao, X. (2017). Mapping plastic greenhouse with medium spatial resolution satellite data: Development of a new spectral index. *ISPRS Journal of Photogrammetry and Remote Sensing*, 128, 47-60. doi:10.1016/j.isprsjprs.2017.03.002

Zhao, G., Li, J., Li, T., Yue, Y., & Warner, T. (2004). Utilizing landsat TM imagery to map greenhouses in Qingzhou, Shandong Province, China. *Pedosphere*, 14(3), 363-369.